Multichromatic Narrow-Energy-Spread Electron Bunches from Laser-Wakefield Acceleration with Dual-Color Lasers

M. Zeng,[1,2] M. Chen,[1,2,*] L. L. Yu,[1,2] W. B. Mori,[3] Z. M. Sheng,[1,2,4,†] B. Hidding,[4] D. A. Jaroszynski,[4] and J. Zhang[1,2]
[1]Key Laboratory for Laser Plasmas (Ministry of Education), Department of Physics and Astronomy, Shanghai Jiao Tong University, Shanghai 200240, China
[2]IFSA Collaborative Innovation Center, Shanghai Jiao Tong University, Shanghai 200240, China
[3]University of California, Los Angeles, California 90095, USA
[4]SUPA, Department of Physics, University of Strathclyde, Glasgow G4 0NG, United Kingdom
(Received 30 June 2014; published 24 February 2015)

A method based on laser wakefield acceleration with controlled ionization injection triggered by another frequency-tripled laser is proposed, which can produce electron bunches with low energy spread. As two color pulses copropagate in the background plasma, the peak amplitude of the combined laser field is modulated in time and space during the laser propagation due to the plasma dispersion. Ionization injection occurs when the peak amplitude exceeds a certain threshold. The threshold is exceeded for limited duration periodically at different propagation distances, leading to multiple ionization injections and separated electron bunches. The method is demonstrated through multidimensional particle-in-cell simulations. Such electron bunches may be used to generate multichromatic x-ray sources for a variety of applications.

DOI: 10.1103/PhysRevLett.114.084801 PACS numbers: 29.25.Bx, 41.75.Jv, 42.55.Vc, 82.53.-k

Versatile x-ray sources with tunable brightness, spectrum range, pulse duration, and temporal-spatial coherence could be tools for scientific discoveries as well as medical and industrial applications. Continuous efforts are being made to push x-ray sources towards new limits such as coherent x rays over 10 keV [1,2], attosecond pulses [3], two-color hard x-ray lasers [4], etc. However, currently most of these sources are based on conventional accelerators. More compact and low cost x-ray devices with comparable quality are highly desired. Recently, laser wakefield acceleration (LWFA) offers the possibility for a new generation of compact particle accelerators [5]. Single or multiple bunches can be generated for different applications [6–8]. LWFA-based compact and low cost x-and γ-ray sources also have attracted much interest [9–12].

In spite of the significant progress made in LWFA research in the past decade [13–18], it is widely recognized that the beam quality and stability still need to be improved considerably before its wide applications. The injection process is a key issue of high quality beam production. There are a few interesting schemes proposed. A cold optical injection scheme is proposed to produce ultralow energy spread beams as shown by two-dimensional (2D) simulations [19]. Besides, ionization-induced injection in mixed gaseous targets has been proposed and demonstrated as an attractive scheme [20–30] due to the relatively easier operation. In this scheme a mixture of gases is chosen. In the mixture, at least one of the gas elements has a relatively low ionization threshold such that it is effectively preionized and acts as background plasma, while at least another has inner shells with higher ionization thresholds (such as nitrogen and oxygen). The laser releases these inner shell electrons at a location within the wake such that they can be easily trapped and accelerated. Generally, the final electron beam energy spread is related to the effective injection length [31–33], which often leads to energy spread much larger than 1%, unless some technique, such as laser self-focusing, is used [34].

In this Letter, we propose a new electron injection scheme to produce ultralow energy spread and single or multiple electron bunches with equally spaced energy peaks. We use a bichromatic laser to trigger sequential ionization injections. In our one-dimensional (1D) and multidimensional particle-in-cell (PIC) simulations using the code OSIRIS [35], low energy spread beams are generated because the effective injection length is suppressed to a few hundred micrometers. A multipeak energy spectrum can also be observed if a specific condition is satisfied.

This scenario is illustrated in Fig. 1. A main pulse with the fundamental frequency is responsible for driving an accelerating wakefield in the blowout regime [36–38]. A second copropagating harmonic pulse with a smaller amplitude modulates the peak laser field strength and acts as a trigger of the high-Z gas K-shell ionization. Because of the laser dispersion in the plasma, the phase speed of the two frequency components are different. By tuning the amplitude of the two components, one can limit the K-shell ionization only occurring when the peaks of the two lasers overlap.

To understand this process, we first study the propagation of a bichromatic laser in plasmas. Consider two plane waves ($i = 1, 2$) with the normalized vector potentials

$$a_i(z,t) = a_{i0}\sin(\omega_i t - k_i z + \phi_i), \tag{1}$$

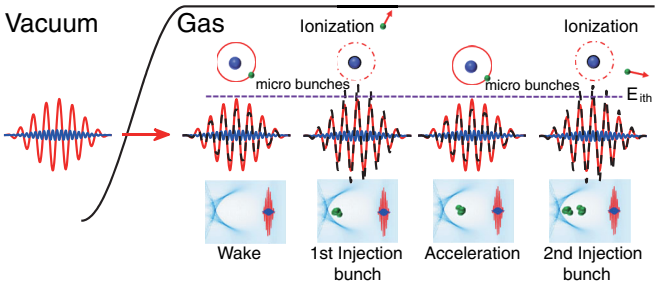

FIG. 1 (color online). Schematic view of dual color lasers trigged periodic injection in LWFA. A laser with base frequency ω_1 (the red curves) and its harmonic ω_2 (the blue curves) propagate in a mixed gas plasma. The dashed black curves show the superposition of the two frequency laser fields at different propagation distances. Laser parameters are chosen so that ionization-induced injection can be switched on when the beating is constructive and be switched off when the beating is destructive. In the plot, $E_{\rm ith}$ represents the effective threshold field for the high-Z gas inner shell ionization.

where a_{i0} are the amplitudes normalized to $m_e c^2/e$, ω_i are the frequencies, k_i are the wave numbers, ϕ_i are the initial phases of the two pulses, respectively. In the linear regime, their frequencies and wave numbers satisfy the linear dispersion relation $\omega_i^2 = \omega_p^2 + c^2 k_i^2$, and for low density plasmas the phase velocity can be expanded as $(\omega_i/k_i) = c[1 - \frac{1}{2}(\omega_p/\omega_i)^2]^{-1}$, where $\omega_p/\omega_i \ll 1$. Substituting these expressions into Eq. (1), rewriting the variables using speed of light frame variables $\xi = \omega_1[t - (z/c)]$ and $s = (\omega_1/c)z$, and normalizing the frequency to ω_1, time to ω_1^{-1}, length to c/ω_1, the laser vector potential can be rewritten as $a_1(\xi, s) = a_{10}\sin(\xi + \frac{1}{2}\omega_p^2 s + \phi_1)$ and $a_2(\xi, s) = a_{20}\sin[\omega_2\xi + \frac{1}{2}(\omega_p^2/\omega_2)s + \phi_2]$. Correspondingly, the electric fields are normalized to $m_e\omega_1 c/e$ and can be written as

$$E_1(\xi, s) = a_{10}\cos\left(\xi + \frac{1}{2}\omega_p^2 s + \phi_1\right),$$
$$E_2(\xi, s) = a_{20}\omega_2\cos\left(\omega_2\xi + \frac{1}{2}\frac{\omega_p^2}{\omega_2}s + \phi_2\right). \quad (2)$$

The total electric field is given by $E(\xi, s) = E_1(\xi, s) + E_2(\xi, s)$. We choose $\omega_2 = 2$, $\omega_p = 0.01$ and $a_{20}/a_{10} = 1/4$ as an example, and the plot is shown in Fig. 2(a). One can find out that changing ϕ_1 and ϕ_2 only leads to shifting the pattern in Fig. 2(a) up and down (or left and right). The period of s over which the beat pattern changes is given by

$$\Delta s = \frac{4\pi}{\omega_p^2(\omega_2 - \frac{1}{\omega_2})}. \quad (3)$$

We only consider the situation that $a_{20} < a_{10}$ and ω_2 to be an integer larger than 1, and optimize the combination of a_{20}/a_{10} and ω_2. Assume the peak field strength of $E(\xi, s)$ for a given s is $E_{\rm peak}(s)$. Its maximum value is found at $s = s_1$ as $E_{\rm peak}|_{\rm max} = E_{\rm peak}(s_1)$ and its minimum value is found at $s = s_2$ as $E_{\rm peak}|_{\rm min} = E_{\rm peak}(s_2)$. Optimization for the controlled ionization injection can be realized by tuning the ratio

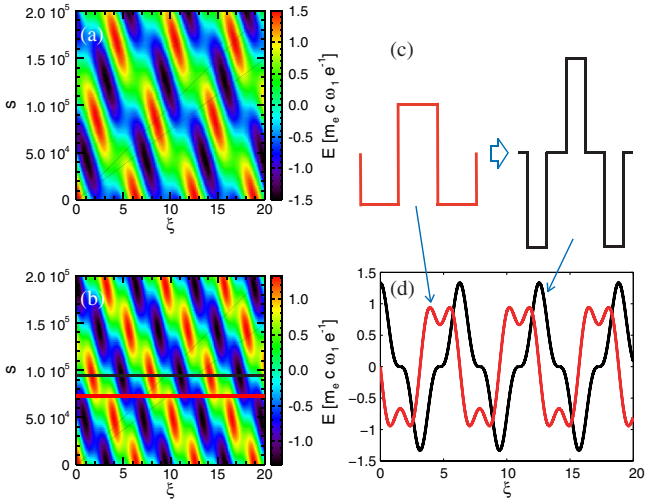

FIG. 2 (color online). Typical evolution of the dual color lasers according to Eq. (2). (a) $a_{10} = 1$, $a_{20} = 1/4$, $\omega_2/\omega_1 = 2$ and $\omega_p/\omega_1 = 0.01$. (b) $a_{10} = 1$, $a_{20} = 1/9$, $\omega_2/\omega_1 = 3$ and $\omega_p/\omega_1 = 0.01$. (c) Illustration showing the reason to use a SWBL combination. (d) Two lineouts of (b) at s values indicated by the black and red lines.

$$R(a_{20}/a_{10}, \omega_2) \equiv E_{\rm peak}|_{\rm max}/E_{\rm peak}|_{\rm min}. \quad (4)$$

It is easy to see that $E_{\rm peak}|_{\rm max} = a_{10} + a_{20}\omega_2$, but it is not straightforward to obtain $E_{\rm peak}|_{\rm min}$ analytically. From Eq. (2) one knows that the dispersion in plasma does not change $\langle E^2(\xi, s)\rangle$ (the power averaged over time ξ), though it changes the peak value of the bichromatic laser field. Consider a square wave at a particular value of s, which has the lowest peak amplitude for a given average power. As the laser evolves the average power remains a constant, but the superposition of the laser components will become narrower peaks as shown in Fig. 2(c). A good approximation of a square wave is the first two components of its Fourier series, i.e., $\omega_2/\omega_1 = 3$ and $a_{20}/a_{10} = 1/9$ as shown in Fig. 2(d). As one can see, using only two frequencies approximates Fig. 2(c) reasonably well. One can verify that the 1:3 combination is optimal by trying other combinations and compare the ratios defined by Eq. (4). We call this combination, the square-wave like bichromatic lasers (SWBL).

Based on the peculiar peak amplitude evolution of the SWBL, the ionization injection region can be broken into small pieces. By choosing the amplitude of the SWBL so that

$$E_{\rm peak}|_{\rm min} < E_{\rm N^{5+}} < E_{\rm peak}|_{\rm max}, \quad (5)$$

the ionization injections can be limited to a few small separated regions, where $E_{N^{5+}}$ is the effective ionization threshold of N^{5+}. One may find $E_{\text{peak}}|_{\max} = \frac{4}{3} a_{10} m_e c \omega_1 e^{-1}$ and $E_{\text{peak}}|_{\min} = \frac{2\sqrt{2}}{3} a_{10} m_e c \omega_1 e^{-1}$.

In Fig. 3 we show the 1D PIC simulation results of such multiple ionization injection and acceleration processes. ω_1 is chosen to be the frequency of the 800 nm laser and $a_{10} = 1.6$. The laser pulse duration is 33 fs in FWHM with the $\sin^2$ profile. The background plasma is provided by helium with the plasma density of $n_p = 1.6 \times 10^{-3} n_c$, where n_c is the critical density of the 800 nm laser. The injection provider is nitrogen with the density of $n_N = 1.6 \times 10^{-7} n_c$. The sequential ionization injections can be found in Fig. 3(a). The curves in Fig. 3(b) show the evolution of the laser peak amplitude predicted by the theory and the result from the simulation. The differences of the theory and the simulation after some propagation distance are due to the plasma response and the nonlinear laser frequency shifting [39]. To control the injection bunch numbers we set the mixed gas length within an appropriate length of 1 mm. These types of gas jets have already been used in several laboratories [32].

Totally, three discrete bunches are observed in this simulation and the energy spectrum at an acceleration distance of 4854.4 μm is shown in Fig. 3(c) with the three peaks labeled, corresponding to the three injections shown in Figs. 3(a) and 3(b) within the mixed gas region. Each injection duration is limited to $100 \sim 200$ μm. In this specific simulation, the second bunch has its minimal

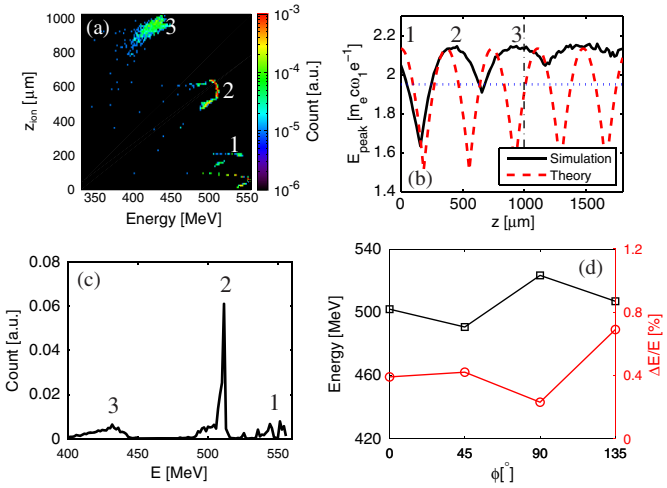

FIG. 3 (color online). 1D PIC simulation of the SWBL and injections. (a) Electron energy at the diagnostic point vs the initial position of the injected electrons. (b) The SWBL peak amplitude evolution. The blue dotted line is the estimated inner shell ionization threshold, and the black dash-dotted line is the separation from the mixed gas to the pure helium gas. (c) Electron beam spectrum at the distance 4860 μm, where the minimum energy spread during the phase rotation is measured to be 0.29% in FWHM. (d) The energy and energy spread in FWHM vs the initial laser phase ϕ.

energy spread of 0.29% at a distance of 4860 μm, while the other two bunches can also get their minimum energy spreads at other appropriate acceleration distances. It is worth noting that even though the optimal acceleration distances for the minimal energy spreads are different for different bunches, this proposed scheme is robust because the accelerated beams can keep a low energy spread in a sufficient wide range of acceleration distances, which is clearer in multidimensional cases.

For such a two-color beat wave ionization injection scheme, the initial phases of the two pulses may affect the specific ionization injection position. Without loss of generality, let $\phi_1 = \phi_2 \equiv \phi$, and change ϕ from 0° to 135°, which correspondingly changes the positions of the electric field reaching $E_{\text{peak}}|_{\max}$. The output beam energies and energy spreads at acceleration distance of 4800 μm are shown in Fig. 3(d). One can see that the central energy of a specific electron bunch at a fixed laser propagation distance has a fluctuation of 30 MeV, which is close to the energy difference between the first and second bunch shown in Fig. 3(c). This energy fluctuation comes from the different injection positions set by the two laser phases. Nevertheless, we find all these simulations show quite good beam quality. They keep small energy spreads of less than 1% regardless of the initial phase change.

Besides the phase effects, other high dimensional effects such as self-focusing, evolution of the bubble radius, and off axis ionizations, may also affect the injection and acceleration. Among them, self-focusing and the associated evolution of the bubble radius are most important. One of the solutions is to choose a matched spot size [38]. Another solution is to choose a relative large spot size so that self-focusing occurs after a sufficiently long acceleration distance, during which multiple injections have already established. Generally, self-focusing occurs in a distance estimated by $z_{\text{sf}} = Z_R[(\alpha/32)a_{10}^2 k_p^2 W_0^2 - 1]^{-1/2}$, where $\alpha = \sqrt{2}$ for a 2D slab geometry and $\alpha = 1$ for a 2D cylindrical or 3D geometry [34,40]. With the presence of self-focusing, a two-stage acceleration process should be deployed [31,32]. For the multiple injection to occur, it is required that the injection stage length satisfies

$$L_{\text{inj}} < z_{\text{sf}}. \tag{6}$$

In this case, the number of ionization injected bunches can be estimated as

$$N_{\text{bunch}} = \left[L_{\text{inj}} / \left(\frac{c\Delta s}{\omega_1} \right) \right], \tag{7}$$

where the square brackets pair means the downward rounding. The energy difference between the monoenergetic peaks can be estimated by the injection position difference times the averaged acceleration gradient

$$\Delta\text{Energy} = \frac{c\Delta s}{\omega_1} \times \frac{1}{2} G_0, \tag{8}$$

where $G_0[\text{eV/m}] \approx 96\sqrt{n_p[\text{cm}^{-3}]}$.

A typical 2D simulation is shown in Fig. 4, where we choose $a_{10} = 1.46$, $a_{20} = 0.162$, $W_0 = 80$ μm, and the other parameters are the same as those in the 1D simulations. The initial laser amplitude in the 2D simulation is lower than that in one dimension. But when the SWBL field reaches its first maximum in two dimensions, the peak field strength is very close to that in the 1D cases due to the self-focusing effect. The injection stage length is $L_{\text{inj}} = 1$ mm so that Eq. (6) is satisfied. A typical distribution of the injected bunches is shown in Fig. 4(a). The central positions of these bunches are spatially separated at this snapshot with μm scale separations. Figure 4(b) shows the phase space distribution of the bunches, from which we see within the second and the third bunches there are a few microbunches. These microbunches come from the several overlapping peaks of the combined electric fields larger than the ionization threshold as schematically shown in Fig. 1. These bunches degrade the monochromaticity of the final beams, showing the pedestals between the peaks of the energy spectrum in Fig. 4(c). In addition, the whole spectrum is composed of three main peaks with the separation of 30 MeV confirming the prediction of Eqs. (7) and (8). From our simulations we find these pedestals can be reduced by using a shorter 3ω laser, which makes the inner shell ionization only occur in a single overlapping electric field peak. A simulation with a 10 fs 3ω laser gives a single injected electron bunch with final energy spread less than 0.2% in FWHM.

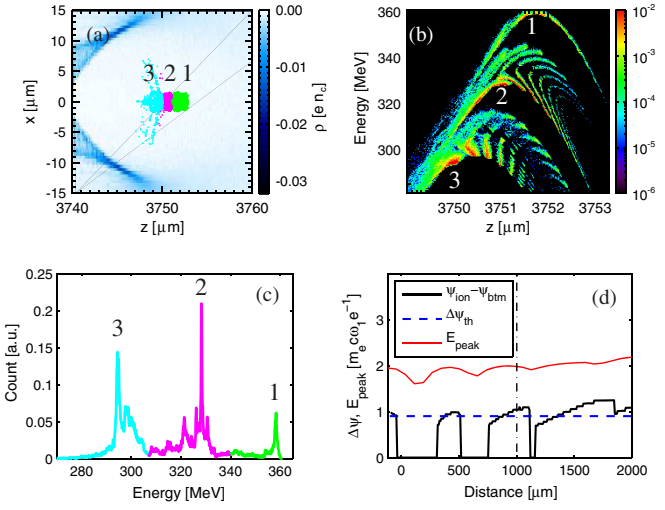

FIG. 4 (color online). 2D PIC simulations of the SWBL injection scheme. (a) The density snapshot at $z = 3780$ μm. The colored dots show the locations of three electron bunches. (b) The energy and space distribution of the energetic electrons. (c) The spectrum of the injected electrons, showing three monoenergetic peaks. (d) The pseudopotential (ψ) difference of the wake and the laser peak field evolution. The dash-dotted line is the separation from the mixed gas region to the pure helium region.

The injection positions of the electrons can be estimated by evaluating both the ionization threshold and the pseudopotential (ψ) differences [23] related to the wake and the ionized electrons. The threshold for ionization injection is given by $\Delta\psi_{\text{th}} = 1 - [\sqrt{1 + (p_\perp/m_e c)^2}/\gamma_{\text{ph}}] \approx 0.9$, where the normalized transverse momentum is estimated to be the normalized laser vector potential at ionization $p_\perp/m_e c \approx 1.9$, and the wake phase velocity Lorentz factor is estimated by the linear theory $\gamma_{\text{ph}} \approx \omega/\omega_p = 25$. In Fig. 4(d), the blue dashed line shows this threshold, and the black line shows the drop of ψ from the nitrogen K-shell ionization position to the minimum ψ, which is manually set to zero when the laser amplitude is lower than the K-shell ionization threshold. There are three periods in the injector region (distance up to 1000 μm) that satisfy the injection condition, consistent with the three period when the laser peak field exceeds the effective ionization threshold of the nitrogen inner shell, and also is consistent with the three injected bunches. In the simulation, we found that within a larger distance (between 3.5 and 4.5 mm), all of the bunches keep very low energy spread (less than 0.4% in FWHM). This gives a very larger acceleration distance window to get a high quality beam in experiments.

A series of 3D simulations are also performed. A typical result is shown in Fig. 5, in which we choose $n_p = 8 \times 10^{-4} n_c$, $a_{10} = 1.485$, $W_0 = 40$ μm, and $L_{\text{inj}} = 1$ mm so that $N_{\text{bunch}} = 1$ according to Eq. (7). A beam with a total charge of 12.6 pC, a mean energy of 389 MeV, and a true root mean squareenergy spread of 1.53% is produced, which confirms the effectiveness of the SWBL injection scheme. From other 3D simulations we notice that as n_p decreases (laser power should be no less than the critical power for self-guiding while keeping a_0 unchanged, thus W_0 may be increased accordingly), the laser can be self-guided longer, the final electron beam energy increases, and the relative energy spread decreases. Although we have not yet tested the GeV level acceleration due to the limited computational resources available, from the serial 3D runs

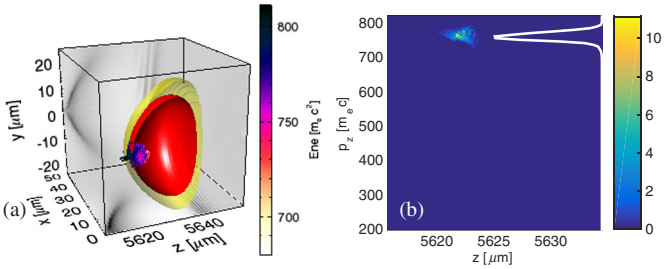

FIG. 5 (color online). A 3D PIC simulation of the SWBL injections. (a) A 3D wake plot. Only a half of the bubble is plotted to show the inner structure of the bubble and the injected electrons. The electron beam has normalized emittances of 3.3 μm rad in the laser polarization direction, and 2.3 μm rad in the perpendicular direction. (b) Phase space of the injected charge. The white curve is the projection to the p_z axis.

with absolute energy spread ~5 MeV it is very promising that our injection scheme can produce electron beams with energy spread lower than 1% once the plasma density and laser power are suitable for GeV level accelerations.

In conclusion, we have proposed a dual color laser scheme to control ionization injection in LWFAs. It can result in periodic triggering of the ionization injection and consequently produce a unique comblike energy spectrum. These features are demonstrated by multidimensional PIC simulations. The energy spread of an individual electron bunch produced from a single injection period can be controlled down to around 1% or even less with the central energy of a few hundred MeV. Our scheme to generate multichromatic narrow energy-spread electron bunches can be used for multi color x-ray generation [4,41], which is particularly interesting for medical imaging applications [42,43]. The multichromatic beams may also be interesting for radiotherapy [44].

This work was supported by the National Basic Research Program of China (No. 2013CBA01504), the National Natural Science Foundation of China (Nos. 11421064, 11374209, 11374210, and 11405107), the MOST international collaboration project (No. 2014DFG02330). M. C. appreciates the support from National 1000 Youth Talent Project of China. W. B. M. acknowledges the support of the US DOE DE-SC 0008491, DE SC 0008316, DE FG02 92ER401727 and the US NSF ACI 1339893. D. A. J. acknowledges the support of the UK EPSRC (No. EP/J018171/1), the EU FP7 programmes: the ELI project, the Laserlab-Europe (No. 284464), and the EUCARD-2 Project (No. 312453). The authors would like to acknowledge the OSIRIS Consortium, consisting of UCLA and IST (Lisbon, Portugal) for the use of OSIRIS and the visXD framework. Simulations were carried out on the Π supercomputer at Shanghai Jiao Tong University.

*minchen@sjtu.edu.cn
†zmsheng@sjtu.edu.cn

[1] T. Ishikawa *et al.*, Nat. Photonics **6**, 540 (2012).
[2] P. Emma *et al.*, Nat. Photonics **4**, 641 (2010).
[3] F. Krausz and M. Ivanov, Rev. Mod. Phys. **81**, 163 (2009).
[4] T. Hara *et al.*, Nat. Commun. **4**, 2919 (2013).
[5] T. Tajima and J. M. Dawson, Phys. Rev. Lett. **43**, 267 (1979).
[6] A. Oguchi, A. Zhidkov, K. Takano, E. Hotta, K. Nemoto, and K. Nakajima, Phys. Plasmas **15**, 043102 (2008).
[7] S. Corde, C. Thaury, A. Lifschitz, G. Lambert, K. Ta Phuoc, X. Davoine, R. Lehe, D. Douillet, A. Rousse, and V. Malka, Nat. Commun. **4**, 1501 (2013).
[8] O. Lundh, C. Rechatin, J. Lim, V. Malka, and J. Faure, Phys. Rev. Lett. **110**, 065005 (2013).
[9] S. Chen *et al.*, Phys. Rev. Lett. **110**, 155003 (2013).
[10] S. Cipiccia *et al.*, Nat. Phys. **7**, 867 (2011).
[11] K. T. Phuoc, S. Corde, C. Thaury, V. Malka, A. Tafzi, J. P. Goddet, R. C. Shah, S. Sebban, and A. Rousse, Nat. Photonics **6**, 308 (2012).
[12] S. Corde, K. Ta Phuoc, G. Lambert, R. Fitour, V. Malka, A. Rousse, A. Beck, and E. Lefebvre, Rev. Mod. Phys. **85**, 1 (2013).
[13] W. P. Leemans, B. Nagler, A. J. Gonsalves, Cs. Tóth, K. Nakamura, C. G. R. Geddes, E. Esarey, C. B. Schroeder, and S. M. Hooker, Nat. Phys. **2**, 696 (2006).
[14] E. Esarey, C. B. Schroeder, and W. P. Leemans, Rev. Mod. Phys. **81**, 1229 (2009).
[15] V. Malka, Phys. Plasmas **19**, 055501 (2012).
[16] S. Hooker, Nat. Photonics **7**, 775 (2013).
[17] X. Wang *et al.*, Nat. Commun. **4**, 1988 (2013).
[18] K. Nakajima *et al.*, Chin. Optic. Lett. **11**, 013501 (2013).
[19] X. Davoine, E. Lefebvre, C. Rechatin, J. Faure, and V. Malka, Phys. Rev. Lett. **102**, 065001 (2009).
[20] M. Chen, Z.-M. Sheng, Y.-Y. Ma, and J. Zhang, J. Appl. Phys. **99**, 056109 (2006).
[21] E. Oz *et al.*, Phys. Rev. Lett. **98**, 084801 (2007).
[22] C. McGuffey *et al.*, Phys. Rev. Lett. **104**, 025004 (2010).
[23] A. Pak, K. A. Marsh, S. F. Martins, W. Lu, W. B. Mori, and C. Joshi, Phys. Rev. Lett. **104**, 025003 (2010).
[24] C. E. Clayton *et al.*, Phys. Rev. Lett. **105**, 105003 (2010).
[25] B. Hidding, G. Pretzler, J. B. Rosenzweig, T. Königstein, D. Schiller, and D. L. Bruhwiler, Phys. Rev. Lett. **108**, 035001 (2012).
[26] F. Li *et al.*, Phys. Rev. Lett. **111**, 015003 (2013).
[27] N. Bourgeois, J. Cowley, and S. M. Hooker, Phys. Rev. Lett. **111**, 155004 (2013).
[28] L.-L. Yu, E. Esarey, C. B. Schroeder, J.-L. Vay, C. Benedetti, C. G. R. Geddes, M. Chen, and W. P. Leemans, Phys. Rev. Lett. **112**, 125001 (2014).
[29] X. L. Xu *et al.*, Phys. Rev. ST Accel. Beams **17**, 061301 (2014).
[30] M. Chen *et al.*, Phys. Rev. ST Accel. Beams **17**, 051303 (2014).
[31] B. B. Pollock *et al.*, Phys. Rev. Lett. **107**, 045001 (2011).
[32] J. S. Liu *et al.*, Phys. Rev. Lett. **107**, 035001 (2011).
[33] M. Chen, E. Esarey, C. B. Schroeder, C. G. R. Geddes, and W. P. Leemans, Phys. Plasmas **19**, 033101 (2012).
[34] M. Zeng, M. Chen, Z.-M. Sheng, W. B. Mori, and J. Zhang, Phys. Plasmas **21**, 030701 (2014).
[35] R. A. Fonseca *et al.*, *Lecture Notes in Computer Science* (Springer, New York, 2002), Vol. 2331, p. 342.
[36] A. Pukhov and J. Meyer-ter Vehn, Appl. Phys. B **74**, 355 (2002).
[37] W. Lu, C. Huang, M. Zhou, W. B. Mori, and T. Katsouleas, Phys. Rev. Lett. **96**, 165002 (2006).
[38] W. Lu, M. Tzoufras, C. Joshi, F. Tsung, W. Mori, J. Vieira, R. Fonseca, and L. Silva, Phys. Rev. ST Accel. Beams **10**, 061301 (2007).
[39] C. D. Murphy *et al.*, Phys. Plasmas **13**, 033108 (2006).
[40] K.-C. Tzeng and W. B. Mori, Phys. Rev. Lett. **81**, 104 (1998).
[41] A. Marinelli, A. A. Lutman, J. Wu, Y. Ding, J. Krzywinski, H.-D. Nuhn, Y. Feng, R. N. Coffee, and C. Pellegrini, Phys. Rev. Lett. **111**, 134801 (2013).
[42] C. Paulus, J. Tabary, N. Billon Pierron, J.-M Dinten, E. Fabiani, F. Mathy, F. Mougel, J. Rinkel, and L. Verger, JINST **8**, P04003 (2013).
[43] B. Dierickx, N. Buls, C. Bourgain, C. Breucq, J. Demey, B. Dupont, and A. Defernez, *On the Diagnostic Value of Multi-energy X-ray Imaging for Mammography* (European Optical Society, Munich, 2009).
[44] V. Malka, J. Faure, Y. A. Gauduel, E. Lefebvre, A. Rousse, and K. Ta Phuoc, Nat. Phys. **4**, 447 (2008).